

Stability of flow in a wavy channel

By A. CABAL†, J. SZUMBARSKI AND J. M. FLORYAN

Department of Mechanical and Material Engineering, The University of Western Ontario,
London, Ontario, N6A 5B9, Canada

(Received 2 October 2000 and in revised form 11 September 2001)

Linear stability analysis of flow in a channel bounded by wavy walls is considered. It is shown that wall waviness gives rise to an instability that manifests itself through generation of streamwise vortices. The available results suggest that the critical stability criteria based on the Reynolds number based on the amplitude of the waviness can be formulated.

1. Introduction

Rough walls exist in all flow systems, where they may lead either to deterioration or improvement of the desired functionality. Nature provides numerous instances where rough surfaces are essential for the survival of many species of air and marine animals. For instance, as noted by Bechert (1987), shark scales have humplets, so spatial variations in their placement should lead to at least as good a drag reduction as that found for streamwise aligned riblets by Chu & Karniadakis (1993).

Wall roughness can be increased to promote mixing of the fluid, or reduced to eliminate flow disturbances. The related problem of the laminar–turbulent transition over a rough wall is one of the classical problems in fluid mechanics that has so far defied all analytical efforts. Qualitative understanding of the mechanisms through which surface roughness may affect transition is of considerable practical importance, it touches almost every field of fluid dynamics from biology to aeronautics.

Some experiments (Feindt 1956; Kendall 1981; Reshotko & Leventhal 1981; Reshotko 1984; Corke, Bar Sever & Morkovin 1986) have shown that roughness enhances transition in the sense that under otherwise identical conditions transition occurs at a lower Reynolds number on a rough surface than on a smooth surface. The existence of roughness elements gives rise to additional disturbances in the laminar stream which have to be added to those coming from the environment. If disturbances created by the roughness elements are larger than those coming from the environment, we should expect that a lower degree of amplification will be sufficient to effect the transition. On the other hand, if the roughness height is sufficiently small, it has no effect on the transition process; the corresponding walls are considered to be hydraulically smooth. Ability of roughness elements to significantly alter transition depends, beside their size, on their geometrical form and their distribution. The real challenge is to identify mechanisms through which surface roughness may affect transition and to provide conservative transition prediction criteria that can be used in the case of roughness-sensitive engineering designs.

† Current address: Integrated Materials and Microstructures, Hardcopy and Display Technology Division, Research Labs, Eastman Kodak Company, Rochester, NY 14650-2121, USA.

Analysis of flows over rough/corrugated boundaries is conditional upon availability of algorithms capable of determining spectral composition of flow with spectral accuracy. The available approaches can be divided into two categories. In the first one, the irregular flow domain is mapped onto a regular computational domain. Imposition of the flow boundary conditions becomes simple; however, we have to work with a much more complex form of the flow field equations. In the second approach, we work directly in the physical domain. The field equations have a very simple form; however, we have to develop special procedures for the imposition of boundary conditions.

The effect of the presense of roughness can be judged by analysing the change in the behaviour of small disturbances in the roughness modified flow as compared to the flow over a smooth wall. Growth of small disturbances in the case of a smooth channel is described by the classical linearized operator; this growth can have two forms. The asymptotic growth (as $t \rightarrow \infty$) is described by the eigenvalues of this operator. The flow is considered to be stable if there are no unstable eigenvalues. Even if all eigenvalues are stable, the disturbances can be subject to initial growth, so-called transient growth, owing to the interdependence of various modes associated with the non-normality of the operator. This transient growth may be sufficient to bring disturbances to the level where they can trigger a by-pass transition. These issues are discussed by Schmid & Henningson (2001). Presence of roughness is expected to modify the above processes. Roughness can also introduce new forms of flow response not found in the case of the smooth channel. The goal of the present analysis is to determine how the roughness affects the asymptotic (as $t \rightarrow \infty$) growth of disturbances. The normal modes approach is used and the problem is posed as an eigenvalue problem.

The paper is organized as follows. Section 2 describes the reference flow and a method based on domain transformation (DTM). Section 3 describes the linear stability problem of the modified Poiseuille flow using DTM and carries out the stability analysis for a test problem with upper and lower roughness described by one Fourier harmonic. Section 4 discusses the linear stability characteristics of the above flow. In §5, a short summary of our main conclusions is given.

2. Flow in a corrugated channel

This section describes a method for determination of the form of the flow in the corrugated channel

2.1. Reference flow

Consider plane Poiseuille flow confined between flat rigid walls at $y = \pm 1$ and extending to infinity in the x -direction (figure 1a). The fluid motion is described by the following velocity and pressure fields

$$\mathbf{v}_0(x, y) = [u_0(x, y), v_0(x, y)] = [U(y), 0] = [1 - y^2, 0], \quad (2.1)$$

$$p_0(x, y) \equiv P_0(x) = -\frac{2x}{Re}, \quad (2.2)$$

where the fluid is directed towards the positive x -axis and the Reynolds number Re is based on the half-channel height (L) and the maximum x -velocity (U_{max}). This flow is driven by a constant pressure gradient.

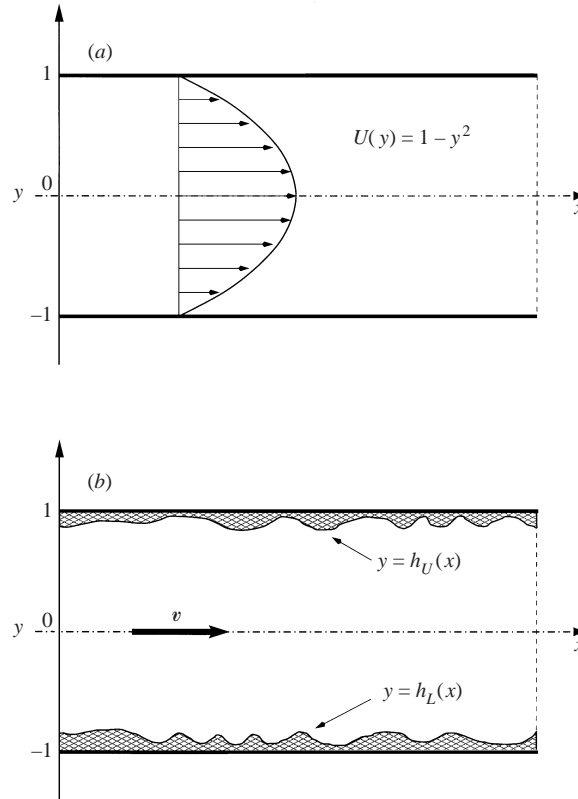


FIGURE 1. Sketch of the flow domain. (a) Straight (reference) channel, (b) channel with corrugated walls.

It is convenient to introduce another reference flow in the form

$$\mathbf{v}_0(x, y) = [u_0(x, y), v_0(x, y)] = [U(y), 0] = \left[\frac{1}{1-\gamma} - \frac{y^2}{(1-\gamma)^3}, 0 \right], \quad (2.3)$$

$$p_0(x, y) \equiv P_0(x) = -\frac{2x}{Re(1-\gamma)^3}. \quad (2.4)$$

This is a Poiseuille flow confined between walls $y = \pm(1-\gamma)$ that carries the same mass flux as the flow (2.1)–(2.2). Flow (2.3)–(2.4) is convenient for discussion of the effects of simple wall displacement.

2.2. Effects of wall corrugations

Consider the upper and lower walls to have arbitrary shapes described by $h_U(x)$ and $h_L(x)$ (figure 1b), respectively, and characterized by certain periodicity with wavelength $\lambda_x = 2\pi/\alpha$. The shape of the walls can be expressed in terms of a Fourier series in the form

$$h_U(x) = 1 + \sum_{n=-\infty}^{+\infty} (A_n)_U e^{in\alpha x}, \quad h_L(x) = -1 + \sum_{n=-\infty}^{+\infty} (A_n)_L e^{in\alpha x}, \quad (2.5)$$

where $(A_n)_U = (A_n)_U^*$ and $(A_n)_L = (A_n)_L^*$ in order for $h_U(x)$ and $h_L(x)$ to be real, and an asterisk denotes the complex conjugate. The subscripts L and U refer to the lower and upper walls, respectively. The effect of corrugations occurs due to (i) the change

of the mean location of the walls (as described by $(A_o)_L$ and $(A_o)_U$), and (ii) changes in the shape of the walls (described by $(A_n)_L$ and $(A_n)_U$, $n \neq 0$). For example, when both walls are displaced inward by distance γ , the reference flow assumes the form (2.3)–(2.4) rather than (2.1)–(2.2). Obviously, form (2.3)–(2.4) does not account for changes in the geometry of the walls.

The fluid motion in the corrugated channel is described by the following velocity and pressure fields

$$\begin{aligned} \mathbf{v}_2(x, y) &= [u_T(x, y), v_T(x, y)] = \mathbf{v}_0(x, y) + \mathbf{v}_1(x, y) \\ &= [U(y), 0] + [u(x, y), v(x, y)], \end{aligned} \quad (2.6)$$

$$p(x, y) = P_0(x) + p_1(x, y), \quad (2.7)$$

where \mathbf{v}_0 and P_0 denote the velocity and pressure fields associated with the flow in the reference channel, \mathbf{v}_1 and p_1 stand for the velocity and pressure field modifications associated with the presence of the wall corrugation, and u_T and v_T denote the total x and y velocity components, respectively.

The velocity and pressure fields satisfy the Navier–Stokes and continuity equations subject to the following boundary conditions

$$\mathbf{v}_2(x, h_U(x)) = 0, \quad \mathbf{v}_2(x, h_L(x)) = 0. \quad (2.8)$$

Introduction of the stream function

$$u = \frac{\partial \psi}{\partial y}, \quad v = -\frac{\partial \psi}{\partial x}, \quad (2.9)$$

and elimination of pressure, result in the following equation for ψ

$$\left[\left(U + \frac{\partial \psi}{\partial y} \right) \frac{\partial}{\partial x} - \frac{\partial \psi}{\partial x} \frac{\partial}{\partial y} \right] \Delta \psi - \frac{d^2 U}{dy^2} \frac{\partial \psi}{\partial x} = \frac{1}{Re} \Delta(\Delta \psi), \quad (2.10)$$

where Δ denotes the Laplace operator.

The problem formulation has to be completed by specifying two additional conditions for ψ at the walls. In the present analysis, problem (2.8)–(2.10) is closed under the assumption that the volume flux in the corrugated channel is the same as the volume flux in the reference (smooth) channel, i.e.

$$\Psi(h_L(x)) + \psi(x, h_L(x)) = B \quad (B \text{ is an arbitrary constant}), \quad (2.11)$$

$$\Psi(h_U(x)) + \psi(x, h_U(x)) = B + Q \quad (Q \text{ is the volume flux}), \quad (2.12)$$

where Ψ denotes the streamfunction corresponding to the plane Poiseuille flow ($Q = \frac{4}{3}$, $\Psi(-1 + \gamma) = 0$). In all test calculations presented in this paper, constant B was taken to be zero.

2.3. Domain transformation

We shall deal with the difficulties due to the presence of irregular boundaries by mapping the physical domain into a rectangular computational domain as shown in figure 2. Here, we use an analytical mapping in the form

$$\xi = x, \quad \eta = 2 \frac{(y - h_U(x))}{h_U(x) - h_L(x)} + 1, \quad (2.13)$$

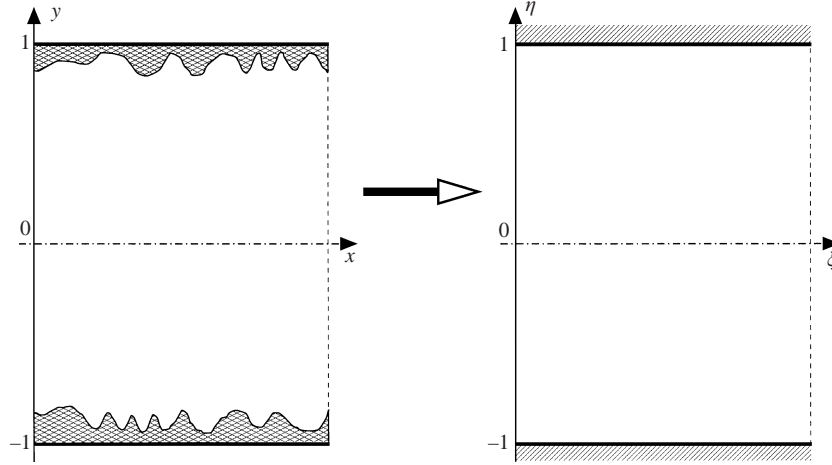


FIGURE 2. Mapping from physical to computational domain. (a) Physical domain, (b) Transformed domain.

in order to avoid additional errors associated with numerical mappings. Equation (2.10) becomes

$$\left\{ \Delta - \text{Re} \left[\left(U + \frac{2}{h_U - h_L} \frac{\partial \psi}{\partial \eta} \right) \left(\frac{\partial}{\partial \xi} + a_{12} \frac{\partial}{\partial \eta} \right) - \frac{2}{h_U - h_L} \times \left(\frac{\partial \psi}{\partial \xi} + a_{12} \frac{\partial \psi}{\partial \eta} \right) \frac{\partial}{\partial \eta} \right] \right\} \Delta \psi + \frac{4 \text{Re}}{(h_U - h_L)^2} \frac{\partial^2 U}{\partial \eta^2} \left(\frac{\partial \psi}{\partial \xi} + a_{12} \frac{\partial \psi}{\partial \eta} \right) = 0, \quad (2.14)$$

where the forms of the coefficients and differential operators are given in Appendix A. The adherence condition at the boundaries is given by

$$\frac{\partial \psi}{\partial \xi} = \frac{1}{2} a_{12} (h_U - h_L) U, \quad \frac{\partial \psi}{\partial \eta} = -\frac{1}{2} (h_U - h_L) U \quad (\eta = \pm 1). \quad (2.15)$$

Notice that the stream function definition (2.9) is not changed. In the (ξ, η) -coordinates it has the form

$$u = \frac{2}{h_U - h_L} \frac{\partial \psi}{\partial \eta}, \quad v = - \left(\frac{\partial \psi}{\partial \xi} + a_{12} \frac{\partial \psi}{\partial \eta} \right). \quad (2.16)$$

Since the shape of the walls is given by (2.5), it is convenient to represent Poiseuille flow and the corresponding streamfunction Ψ in terms of Fourier expansions in the form

$$U(\xi, \eta) = \sum_{n=-\infty}^{+\infty} U_n(\eta) e^{inx\xi}, \quad \Psi(\xi, \eta) = \sum_{n=-\infty}^{+\infty} \hat{\Psi}_n(\eta) e^{inx\xi}, \quad (2.17)$$

where expressions for $U_n, \hat{\Psi}_n$ are given in Appendix B.

The unknown streamfunction can be represented as

$$\psi(\xi, \eta) = \sum_{n=-\infty}^{+\infty} \Phi_n(\eta) e^{inx\xi}. \quad (2.18)$$

Substitution of (2.16) and (2.18) into boundary conditions (2.8) and separation of

Fourier modes results in boundary conditions for each mode in the form

$$\Phi'_n = -U_n - \frac{1}{2} \sum_{k=-\infty}^{+\infty} B_k U_{n-k} \quad (n \geq 0, \quad \eta = \pm 1), \quad (2.19)$$

$$\begin{aligned} 2in\alpha\Phi_n + \sum_{k=-\infty}^{+\infty} i(n-k)\alpha B_k \Phi_{n-k} = & - \sum_{k=-\infty}^{+\infty} [2ik\alpha(A_k)_U + 2ik\alpha B_k] U_{n-k} \\ & - \sum_{m=-\infty}^{+\infty} \sum_{k=-\infty}^{+\infty} [ik\alpha(A_k)_U + ik\alpha B_k] B_m U_{n-m-k} \quad (n \geq 1, \quad \eta = -1), \end{aligned} \quad (2.20)$$

$$\begin{aligned} 2in\alpha\Phi_n + \sum_{k=-\infty}^{+\infty} i(n-k)\alpha B_k \Phi_{n-k} = & - \sum_{k=-\infty}^{+\infty} 2ik\alpha(A_k)_U U_{n-k} \\ & - \sum_{m=-\infty}^{+\infty} \sum_{k=-\infty}^{+\infty} ik\alpha(A_k)_U B_m U_{n-m-k} \quad (n \geq 1, \quad \eta = 1), \end{aligned} \quad (2.21)$$

where $B_n = (A_n)_U - (A_n)_L$. The fixed volume flux condition leads to conditions in the form

$$\Phi_0(-1) = 0, \quad \Phi_0(1) = \frac{4}{3} - \hat{\Psi}_0(1) + \hat{\Psi}_0(-1). \quad (2.22)$$

Substitution of (2.18) into field equation (2.14) and separation of Fourier components leads to an infinite system of complex ordinary differential equations. Because of the length of these equations, their explicit form will not be given. The entire set of equations is described in Cabal (1998).

All numerical calculations discussed in this section have been carried out for the upper and lower walls in the form

$$\left. \begin{aligned} -(A_0)_U = (A_0)_L = \gamma, \quad (A_1)_U = (A_1)_L = s, \\ (A_n)_U = (A_n)_L = 0 \quad \text{for } n \geq 2, \end{aligned} \right\} \quad (2.23)$$

i.e. both walls have identical, symmetric corrugations described by cosine function with amplitude $2s$ and with mean location moved into the channel by distance γ . For this particular case, the Fourier representation (2.17) of the Poiseuille flow has the form

$$\begin{aligned} U_0 = \frac{1}{1-\gamma} - \frac{2s^2}{(1-\gamma)^3} - \frac{\eta^2}{1-\gamma}, \quad U_1 = -\frac{2s\eta}{(1-\gamma)^2}, \\ U_2 = -\frac{s^2}{(1-\gamma)^3}, \quad U_n = 0 \quad (n \geq 3). \end{aligned} \quad (2.24)$$

The differential equations for Φ_n are presented in Appendix C.

2.4. Numerical solution

After truncation of (2.18) to N modes, system (C1)–(C7) is solved using a variable-step-size finite-difference discretization with deferred corrections (see Pereyra 1979; Cash & Wright 1991). The solution strategy used in order to guarantee convergence of the iterative process consists of obtaining at first a solution to the problem when $N = 1$, then these results are used as an initial approximation of the solution for $N = 2$. Solution for $N = 2$ is used as an initial guess of the solution for $N = 3$, and so on. Owing to the nature of the solution around the boundaries, a continuation

procedure had to be employed for $N \geq 2$. All calculations have been carried out with the machine-level accuracy. Details of the method can be found in Cabal, Szumbarski & Floryan (2001).

The contributions of different modes can be assessed by calculating their energy. The energy of mode n is defined as

$$E_n := \frac{\alpha}{4\pi} \int_{-1}^1 \int_{\xi_0}^{\xi_0 + (2\pi/\alpha)} \frac{u_n^2 + v_n^2}{2} d\xi d\eta \quad (2.25)$$

where

$$u_n = \hat{u}_n(\eta) e^{inx\xi} + \text{c.c.}, \quad v_n = \hat{v}_n(\eta) e^{inx\xi} + \text{c.c.}$$

and c.c. stands for complex conjugate. From (2.16) and (2.18), we obtain

$$\hat{u}_n = \frac{1}{1-\gamma} \frac{d\Phi_n}{d\eta}, \quad (2.26)$$

$$\hat{v}_n = -i\alpha n \Phi_n - \frac{i\alpha s}{1-\gamma} \frac{d\Phi_{n+1}}{d\eta} + \frac{i\alpha s}{1-\gamma} \frac{d\Phi_{n-1}}{d\eta}, \quad (2.27)$$

which leads to expressions for energy in the form

$$\begin{aligned} E_0 &= \frac{1}{2} \int_{-1}^1 \frac{u_0^2 + v_0^2}{2} d\eta \\ &= \frac{1}{4(1-\gamma)^2} \int_{-1}^1 \left[\left(\frac{d\Phi_0}{d\eta} \right)^2 + 4\alpha^2 s^2 \left(\text{Im} \left(\frac{d\Phi_1}{d\eta} \right) \right)^2 \right] d\eta \end{aligned} \quad (2.28)$$

and

$$\begin{aligned} E_n &= \frac{1}{2} \int_{-1}^1 (|\hat{u}_n|^2 + |\hat{v}_n|^2) d\eta \\ &= \frac{1}{2} \int_{-1}^1 \left(\frac{1}{(1-\gamma)^2} \left| \frac{d\Phi_n}{d\eta} \right|^2 + \alpha^2 \left| \frac{s}{(1-\gamma)} \frac{d\Phi_{n+1}}{d\eta} \right. \right. \\ &\quad \left. \left. - \frac{s}{(1-\gamma)} \frac{d\Phi_{n-1}}{d\eta} + n\Phi_n \right|^2 \right) d\eta \quad (n \geq 1). \end{aligned} \quad (2.29)$$

Variations of energy of modes 0, 1 and 2 as a function of corrugation amplitude $2s$ are depicted in figure 3 for three different values of the shift parameter γ . All calculations were performed using six modes, i.e. streamfunction expansion (2.18) was truncated at $N = 5$. It can be seen that for $Re = 5000$, mode interaction is rather weak for corrugation amplitudes $2s \leq 10^{-2}$. The flow velocity in the expanded channel ($\gamma = -0.1$) is smaller and thus the corresponding energy levels are lower. The opposite occurs with the reduction of the channel width. Because of the use of the reference flow (2.3), the zero mode describes purely nonlinear effects even for $\gamma \neq 0$.

3. Linear stability

3.1. Problem formulation

Unsteady, three-dimensional disturbances are superimposed on the mean part of the flow (2.6) in the form

$$\mathbf{v} = \mathbf{v}_2(\xi, \eta) + \mathbf{v}_3(\xi, \zeta, \eta, t), \quad (3.1)$$

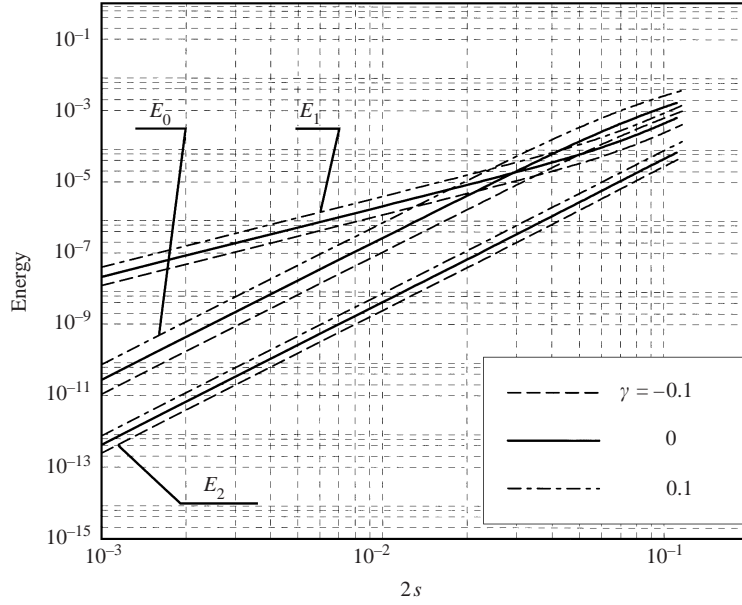


FIGURE 3. Variations of energy of flow modifications induced by wall corrugations as a function of the corrugation amplitude $2s$ for $Re = 5000$, $\alpha = 3.0$, $\gamma = -0.1, 0$ and 0.1 .

where

$$(x, z, y, t) \longrightarrow (\xi, \zeta, \eta, t); \quad (3.2)$$

$$\xi = x, \quad \zeta = z, \quad \eta = 2 \frac{(y - h_U(x))}{h_U(x) - h_L(x)} + 1.$$

Subscripts 2 and 3 refer to the mean flow and the disturbance field, respectively. Defining vorticity in the (ξ, ζ, η) -variables as

$$\boldsymbol{\omega} = \left(\frac{\partial v}{\partial \zeta} - a_0 \frac{\partial w}{\partial \eta}, a_0 \frac{\partial u}{\partial \eta} - \left(\frac{\partial v}{\partial \xi} + a_{12} \frac{\partial v}{\partial \eta} \right), \frac{\partial w}{\partial \xi} + a_{12} \frac{\partial w}{\partial \eta} - \frac{\partial u}{\partial \zeta} \right), \quad (3.3)$$

relations (3.1) and (3.3) yield

$$\boldsymbol{\omega} = \boldsymbol{\omega}_2(\xi, \eta) + \boldsymbol{\omega}_3(\xi, \zeta, \eta, t), \quad (3.4)$$

where

$$\boldsymbol{\omega}_2 = (0, \phi_2, 0), \quad \boldsymbol{\omega}_3 = (\theta_3, \phi_3, \psi_3); \quad (3.5)$$

$$\phi_2 = a_0 \frac{\partial u_2}{\partial \eta} - \left(\frac{\partial v_2}{\partial \xi} + a_{12} \frac{\partial v_2}{\partial \eta} \right),$$

$$\theta_3 = \frac{\partial v_3}{\partial \zeta} - a_0 \frac{\partial w_3}{\partial \eta},$$

$$\phi_3 = a_0 \frac{\partial u_3}{\partial \eta} - \left(\frac{\partial v_3}{\partial \xi} + a_{12} \frac{\partial v_3}{\partial \eta} \right),$$

$$\psi_3 = \frac{\partial w_3}{\partial \xi} + a_{12} \frac{\partial w_3}{\partial \eta} - \frac{\partial u_3}{\partial \zeta},$$

$$a_0(\xi) = \frac{2}{h_U(\xi) - h_L(\xi)},$$

and $a_{12}(\xi, \eta)$ is given in Appendix A. The assumed form (3.1) of the flow field is substituted into the vorticity transport form of the governing equations, the mean part is subtracted and the equations are linearized. The resulting linear disturbance equations have the form

$$\frac{\partial \theta_3}{\partial t} + u_2 \left(\frac{\partial \theta_3}{\partial \xi} + a_{12} \frac{\partial \theta_3}{\partial \eta} \right) - \phi_2 \frac{\partial u_3}{\partial \zeta} + a_0 v_2 \frac{\partial \theta_3}{\partial \eta} - \theta_3 \left(\frac{\partial u_2}{\partial \xi} + a_{12} \frac{\partial u_2}{\partial \eta} \right) - a_0 \psi_3 \frac{\partial u_2}{\partial \eta} = \frac{1}{Re} \Delta \theta_3, \quad (3.6)$$

$$\frac{\partial \phi_3}{\partial t} + u_2 \left(\frac{\partial \phi_3}{\partial \xi} + a_{12} \frac{\partial \phi_3}{\partial \eta} \right) - \phi_2 \frac{\partial w_3}{\partial \zeta} + a_0 v_2 \frac{\partial \phi_3}{\partial \eta} + u_3 \left(\frac{\partial \phi_2}{\partial \xi} + a_{12} \frac{\partial \phi_2}{\partial \eta} \right) + a_0 v_3 \frac{\partial \phi_2}{\partial \eta} = \frac{1}{Re} \Delta \phi_3, \quad (3.7)$$

$$\frac{\partial \psi_3}{\partial t} + u_2 \left(\frac{\partial \psi_3}{\partial \xi} + a_{12} \frac{\partial \psi_3}{\partial \eta} \right) - \phi_2 \frac{\partial v_3}{\partial \zeta} + a_0 v_2 \frac{\partial \psi_3}{\partial \eta} - \theta_3 \left(\frac{\partial v_2}{\partial \xi} + a_{12} \frac{\partial v_2}{\partial \eta} \right) - a_0 \psi_3 \frac{\partial v_2}{\partial \eta} = \frac{1}{Re} \Delta \psi_3, \quad (3.8)$$

$$\frac{\partial u_3}{\partial \xi} + a_{12} \frac{\partial u_3}{\partial \eta} + \frac{\partial w_3}{\partial \zeta} + a_0 \frac{\partial v_3}{\partial \eta} = 0, \quad (3.9)$$

with adherence condition at the boundaries given by

$$u_3 = 0, \quad w_3 = 0, \quad v_3 = 0, \quad \eta = \pm 1. \quad (3.10)$$

In system (3.6)–(3.9), operator Δ is defined by

$$\Delta = \frac{\partial^2}{\partial \xi^2} + 2a_{12}(\xi, \eta) \frac{\partial^2}{\partial \xi \partial \eta} + \frac{\partial^2}{\partial \zeta^2} + a_{22}(\xi, \eta) \frac{\partial^2}{\partial \eta^2} + a_2(\xi, \eta) \frac{\partial}{\partial \eta}. \quad (3.11)$$

It should be noticed that only two of the vorticity equations (3.6)–(3.8) are independent.

In the case of test geometry defined by (2.23), the above equations simplify to the form given in Appendix D.

The mean flow is assumed to have the form

$$\mathbf{v}_2(\xi, \eta) = [U(\eta), 0, V(\eta)] + \{[f_u(\eta), 0, f_v(\eta)]e^{ix\xi} + \text{c.c.}\} + \{[F_u(\eta), 0, F_v(\eta)]e^{2ix\xi} + \text{c.c.}\}, \quad (3.12)$$

i.e. it is limited to the first three modes only. Such description provides means for complete representation of the Poiseuille flow in the transformed domain as well as sufficiently accurate representation of the flow modifications in the case of small amplitudes of surface corrugations, as discussed in § 2.3.

In order to assess the effects of nonlinearities in the basic state on the stability properties of the flow, three representations of the mean flow will be used. When

$N = 1$, flow (3.12) consists of the complete representation of the Poiseuille flow (see (2.17) and (2.24)) and mode $n = 1$ describing flow modifications (see (2.18)). When $N = 0$ and 1, mode corresponding to $n = 0$ in (2.18) is added. When $N = 0, 1$ and 2, modes corresponding to $n = 0, 1$ and 2 from (2.18) are included in (3.12). In each case, (2.18) is truncated at $N = 5$ and the resulting nonlinear system is solved without further approximations (§ 2.4). Particular modes are then extracted for use in the stability analysis, as described above.

The disturbance equations (D 1)–(D 4) have coefficients that are functions of ξ and η only. This permits separation of variables and representation of the t and ζ dependence of the solution in the form

$$\mathbf{v}_3(\xi, \zeta, \eta, t) = \mathbf{u}_3(\xi, \eta) e^{i(\sigma t + \mu \zeta)}. \quad (3.13)$$

The exponent μ is real and accounts for the spanwise periodicity of the disturbance field. The exponent σ is assumed to be complex. Its imaginary part describes the rate of growth of the disturbances while its real part describes the frequency of the disturbances.

Since the coefficients in (D 1)–(D 4) are periodic in ξ with periodicity $2\pi/\alpha$, \mathbf{u}_3 is written, following the Floquet theory, as

$$\mathbf{u}_3(\xi, \eta) = e^{i\delta\xi} \mathbf{w}_3(\xi, \eta) = e^{i\delta\xi} \sum_{m=-\infty}^{+\infty} \mathbf{G}_m(\eta) e^{im\alpha\xi}, \quad (3.14)$$

where \mathbf{w}_3 is periodic in ξ with the same periodicity $2\pi/\alpha$ and δ is referred to as the Floquet exponent. It should be noted that \mathbf{u}_3 is a product of two functions periodic in ξ , one with a period $2\pi/\alpha$ and one with a period $2\pi/\delta$. This product is periodic only if δ/α is rational.

The final form of the disturbance velocity vector is written as

$$\mathbf{v}_3(\xi, \zeta, \eta, t) = \sum_{m=-\infty}^{+\infty} [\mathbf{g}_u^{(m)}(\eta), \mathbf{g}_w^{(m)}(\eta), \mathbf{g}_v^{(m)}(\eta)] e^{i[(\delta+m\alpha)\xi + \mu\zeta + \sigma t]}. \quad (3.15)$$

Substitution of (3.12) and (3.15) into the disturbance equations given in Appendix D and separation of the Fourier components results, after rather lengthy algebra, in a system of linear ordinary differential equations governing $\mathbf{g}_u^{(m)}$, $\mathbf{g}_w^{(m)}$, $\mathbf{g}_v^{(m)}$, whose form is given in Appendix E.

The relevant boundary conditions can be deduced from (3.10), (3.15) and (E 3), i.e.

$$\mathbf{g}_u^{(m)} = 0, \quad \mathbf{g}_v^{(m)} = 0, \quad \mathbf{g}_w^{(m)} = 0 \quad (\eta = \pm 1), \quad (3.16)$$

$$\frac{d}{d\eta} \mathbf{g}_v^{(m)} = i\alpha s \frac{d}{d\eta} \mathbf{g}_u^{(m-1)} - i\alpha s \frac{d}{d\eta} \mathbf{g}_u^{(m+1)} \quad (\eta = \pm 1). \quad (3.17)$$

In the absence of wall corrugation ($s = 0$) all modes from the Fourier series (3.15) decouple and equations (E 1)–(E 3) with boundary conditions (3.16)–(3.17) describe the classical three-dimensional instability of the plane Poiseuille flow. The coupling due to the presence of corrugation effects in the field equations involves eleven consecutive modes of the Fourier expansion (3.15). The coupling due to the presence of corrugation effects in the boundary conditions involves three consecutive modes.

3.2. Computational method

The eigenvalue problem to be solved is described by an infinite set of coupled linear homogeneous ordinary differential equations (E 1)–(E 3) with homogeneous boundary

Number of Chebyshev polynomials	Number of Fourier modes used to represent disturbance field (see (3.15))		
	$M = 0, 1, 2$	$M = 0, 1, 2, 3$	$M = 0, 1, 2, 3, 4$
Number of Fourier modes used to represent flow modifications induced by wall corrugation (see (3.12))			
$N = 1$			
60	0.240×10^{-3}	0.257×10^{-3}	0.249×10^{-3}
70	0.248×10^{-3}	0.243×10^{-3}	0.245×10^{-3}
80	0.238×10^{-3}	0.237×10^{-3}	0.238×10^{-3}
90	0.238×10^{-3}	0.237×10^{-3}	0.238×10^{-3}
Number of Fourier modes used to represent flow modifications induced by wall corrugation (see (3.12))			
$N = 0, 1$			
60	0.199×10^{-3}	0.215×10^{-3}	0.206×10^{-3}
70	0.187×10^{-3}	0.184×10^{-3}	0.185×10^{-3}
80	0.184×10^{-3}	0.184×10^{-3}	0.184×10^{-3}
90	0.185×10^{-3}	0.184×10^{-3}	0.185×10^{-3}
Number of Fourier modes used to represent flow modifications induced by wall corrugation (see (3.12))			
$N = 0, 1, 2$			
60	0.192×10^{-3}	0.229×10^{-3}	0.209×10^{-3}
70	0.186×10^{-3}	0.187×10^{-3}	0.185×10^{-3}
80	0.186×10^{-3}	0.185×10^{-3}	0.186×10^{-3}
90	0.187×10^{-3}	0.184×10^{-3}	0.187×10^{-3}

TABLE 1. Amplification rate $-\text{Im}(\sigma)$ of the corrugation-induced instability for $Re = 5000$, $\gamma = 0$, $2s = 0.014$, $\alpha = 2.0$, $\mu = 2.0$ and $\delta = 0$.

conditions (3.16)–(3.17). Approximate solutions can be found by truncating the sum in (3.15) after a finite number M of terms and solving $6M + 3$ differential equations of type (E 1)–(E 3).

The finite-dimensional system obtained after truncation is discretized by employing a pseudospectral method based on Chebyshev polynomials (see Gottlieb & Orszag 1977; Boyd 1988; Canuto *et al.* 1988; Tang 1994; Fornberg 1996 for comprehensive reviews of the method). The original differential eigenvalue problem is replaced by an algebraic eigenvalue problem expressed in terms of a discretization matrix. In the present analysis, the problem is posed as a linear eigenvalue problem for σ . The σ -spectrum is computed for any combination of parameters Re , α , γ , δ , μ and s using standard methods.

Various test have been carried out in order to determine the minimum mean flow representation (see (3.12)), the minimum truncation M of the disturbance field representation (3.15) and the minimum number of Chebyshev polynomials used for discretization. Table 1 displays the amplification rate $-\text{Im}(\sigma)$ of the corrugation-induced instability as a function of the above parameters. The results show that for the values of corrugation amplitudes of interest in the present study, the eigenvalues can be determined with accuracy no worse than 0.1% using mean flow representation $N = 0, 1$ and 2, disturbance field truncation $M = 3$ and 80 Chebyshev polynomials. These results also show that the mean flow representation with $N = 1$ only (such that could be implied by a linear model of corrugation effects) is not acceptable.

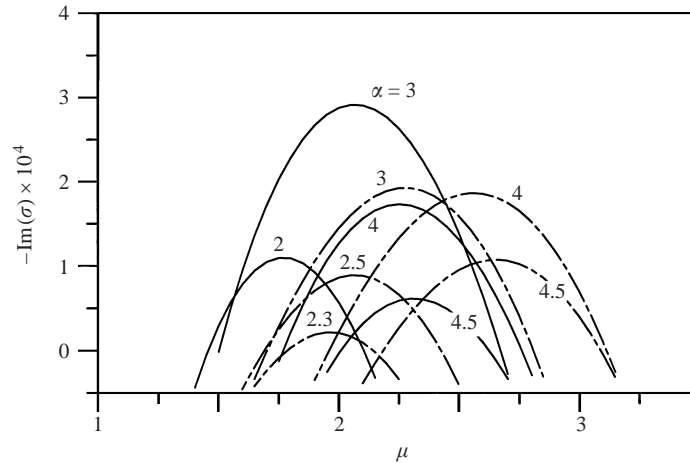


FIGURE 4. Amplification rate $-\text{Im}(\sigma)$ as a function of the spanwise wavenumber μ for the corrugation-induced instability for $Re = 3000$. ---, $2s = 0.02$; —, $2s = 0.022$.

The nonlinear flow distortion corresponding to $N = 0$ plays a significant role in the instability studied here.

4. Discussion of results

We consider temporal stability theory, i.e. the exponent δ in (3.15) is assumed to be real. Exponent μ is real and accounts for the spanwise periodicity of the disturbance field. Exponent σ is complex and its imaginary part describes the rate of growth of the disturbances. All results presented below are for surface corrugation in the form (2.5), (2.23) with $\gamma = 0$, i.e. the corrugation is periodic in the streamwise direction with period $2\pi/\alpha$, it has the form of a simple cosine wave, it is the same at the upper and lower walls, and its presence does not affect the mean location of the walls.

Poiseuille flow in a channel without corrugation becomes linearly unstable at $Re_{TS} = 5772.22$ and the critical disturbance has the form of a two-dimensional wave travelling in the streamwise direction. This wave is frequently referred to as the Tollmien–Schlichting (TS) wave and its critical wavenumber is $\alpha_{cr} \approx 1.0$. Questions to be addressed in this discussion are (i) whether the TS waves dominate the linear instability in the presence of wall corrugation and how much they are affected by the corrugation, and (ii) whether the wall corrugation can induce a different instability that could overshadow the TS waves and what is the form of such an instability.

Results of the present analysis show that the presence of wall corrugation leads to the appearance of growing disturbances at Reynold's number $Re < Re_{TS}$. The disturbances have the form of streamwise vortices, i.e. the dominant mode corresponds to $m = 0$ in (3.15). The disturbances are fixed with respect to the wall and do not propagate, i.e. $\text{Re}(\sigma) = 0$ in (3.15). A whole band of the spanwise wavenumbers μ is amplified and the width of this band increases with an increase of both the corrugation amplitude $2s$ and the flow Reynolds number Re (see figures 4 and 5). Disturbances with $\mu \approx 2.15$ appear to have the largest amplification rates. Corrugation with the wavenumber $\alpha \approx 3$ appears to be the most dangerous in the sense that it induces disturbances with the highest amplification rates.

Appearance of streamwise vortices results in a significant rearrangement and rapid three-dimensionalization of the flow field. Uplifting of low-momentum fluid away

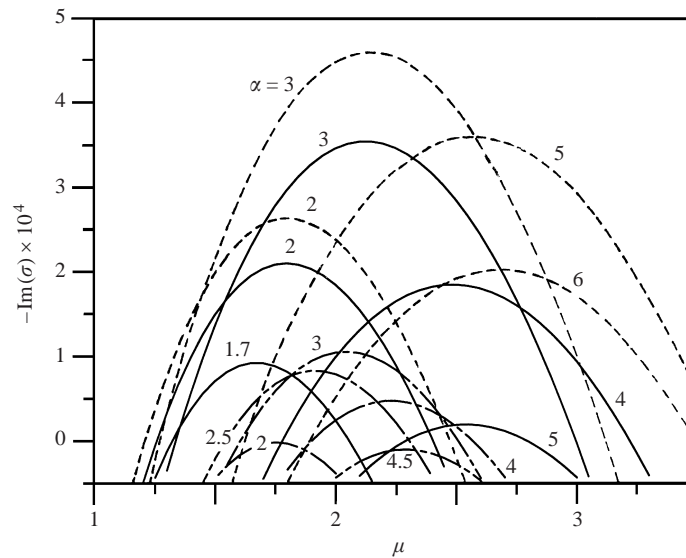


FIGURE 5. Amplification rate $-\text{Im}(\sigma)$ as a function of the spanwise wavenumber μ for the corrugation-induced instability for $Re = 5000$. ---, $2s = 0.013$; —, $2s = 0.014$; - · - ·, $2s = 0.014$ and $N = 1$ ('linear' model).

from the wall leads to the formation of highly distorted streamwise and spanwise velocity profiles that are functions of spanwise and streamwise coordinates and are subject to very strong secondary instabilities. The qualitative character of the instability is very similar to instability induced by periodic suction (Floryan 1997). It has been shown by direct numerical simulation that the suction-induced instability leads to a new (by-pass) route to transition (Floryan, Yamamoto & Murase 1992).

Results displayed in figure 5 and table 1 demonstrate the effect of the use of different models of the mean flow. Use of the one-mode $N = 1$ representation of the mean flow leads to overprediction of the growth rates. The minimum acceptable model consists of modes $N = 0, 1$ and 2 in the range of corrugation amplitudes subject to this investigation. The same conclusion can be deduced from the results shown in figure 3. The flow modifications are more complex as compared to the case of flow modified by periodic suction (Floryan 1997) where only one mode was sufficient to describe flow modifications capable of inducing instability.

Figure 6 displays amplification rates of two-dimensional TS wave with $\alpha = 1$ (critical TS wave) as a function of the Reynolds number Re for different corrugation amplitudes. It can be seen that an increase of corrugation amplitude makes this instability more pronounced. Since these waves are driven by shear, it is the modification of shear due to the presence of wall corrugation that is responsible for the increased amplification.

Modifications of flow due to wall corrugation may create local inflection points in the velocity profile which may activate an inviscid instability mechanism. Careful analysis of the stability spectra failed to identify the presence of any such instability in the range of parameters subject to this investigation.

Figure 6 displays amplification rates for the most amplified vortices ($\alpha = 3, \mu = 2.15$) and critical TS waves ($\alpha = 1$). It can be seen that an increase of the corrugation amplitude destabilizes the flow, the amplification rates of disturbances increase and

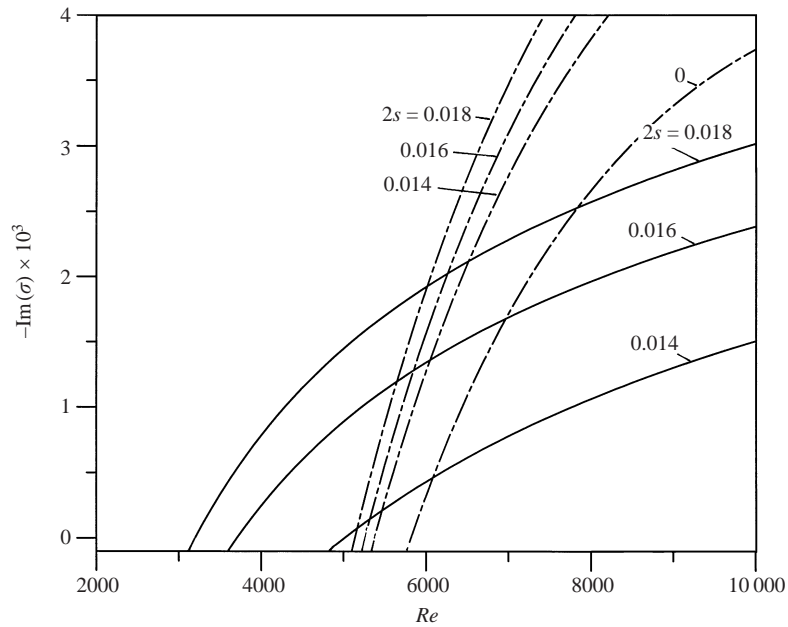


FIGURE 6. Amplification rate $-\text{Im}(\sigma)$ as a function of the Reynolds number Re for the corrugation-induced instability (—, $\mu = 2.15$, $\alpha = 3.0$) and for two-dimensional TS-waves (---, $\mu = 0$, $\alpha = 1.0$).

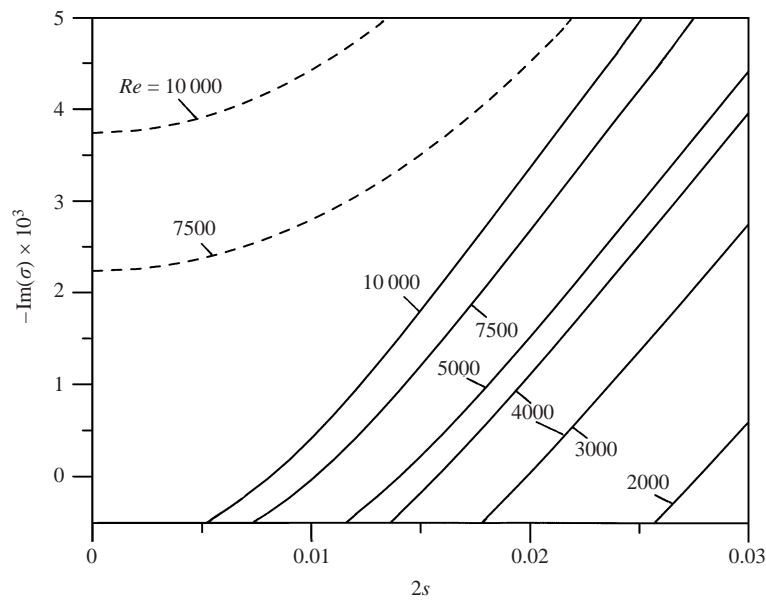


FIGURE 7. Amplification rate $-\text{Im}(\sigma)$ as a function of the corrugation amplitude $2s$ for the corrugation-induced instability (—, $\mu = 2.15$, $\alpha = 3.0$) and for the two-dimensional TS-waves (---, $\mu = 0$, $\alpha = 1.0$).

the minimal Reynolds number at which they appear decreases. Vortices may appear at Reynolds numbers smaller than those required to induce TS waves.

Figure 7 illustrates the effect of corrugation amplitude on the amplification rates of two-dimensional TS waves ($\alpha = 1$) and vortices with $\mu = 2.15$, $\alpha = 3$. An increase of

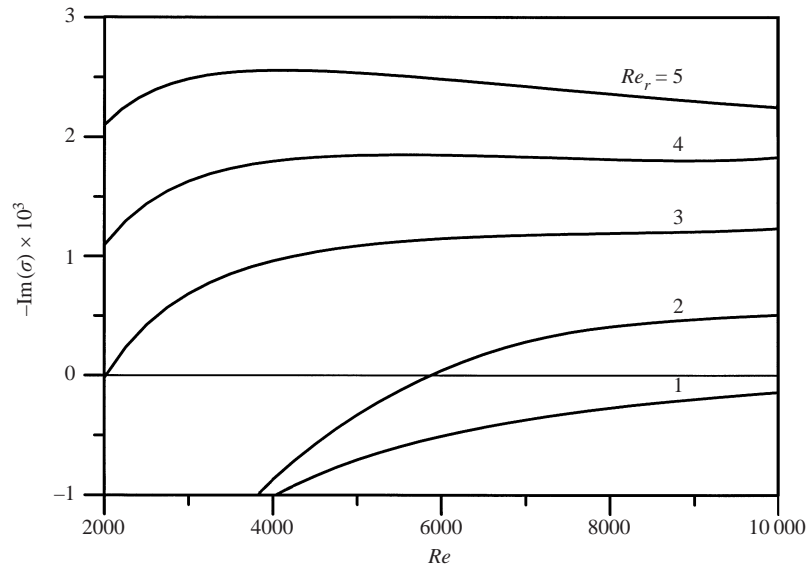


FIGURE 8. Amplification rate $-\text{Im}(\sigma)$ of the corrugation-induced instability as a function of the corrugation Reynolds number Re_r for $\mu = 2.15$, $\alpha = 3.0$.

the amplification rates of TS waves and an almost linear increase of the amplification rates of vortices with increase of $2s$ can be seen clearly. These results also demonstrate that given a particular value of the Reynolds number, we can always find (in the range of parameters studied) a corrugation amplitude that would give rise to streamwise vortices.

Information regarding the maximum corrugation amplitude the flow can accommodate for a given Re without inducing streamwise vortices can be extracted from figures 4–7. The results may be interpreted better by using corrugation Reynolds number defined as $Re_r = U_{tr}2s/\nu = Re8s^2(1-s)$, where U_{tr} stands for the undisturbed velocity at the top of the corrugation. Figure 8 displays variations of the amplification rate of vortices as a function of Reynolds number Re for various values of Re_r for the most amplified disturbances ($\alpha = 3.0$, $\mu = 2.15$). It can be seen that the disturbances are not amplified if $Re_r < 1.2$ (in the range of parameters studied). When $Re_r \leq 3$, the amplification rates increase monotonically with Re and appear to reach an asymptotic value whose magnitude depends on Re_r . For $Re_r > 4$, this trend is reversed in the sense that there is a gradual monotonic decrease of the amplification rates towards their (apparent) asymptotic limit.

5. Conclusions

Stability of Poiseuille flow modified by wall corrugation has been considered. The analysis is focused on a test problem with wall-corrugation in the form of a single two-dimensional Fourier mode with the same shape at the upper and lower walls. The analysis consists of two parts, i.e. (i) determination of the new corrugation-modified flow, and (ii) a linear stability analysis of this flow.

Results of linear stability analysis show the existence of two modes of instability. The first mode gives rise to streamwise vortices and is induced by wall waviness. Such vortices are asymptotically stable (in the sense of eigenvalue analysis) in the absence

of wall waviness. The second mode gives rise to travelling-wave instability. These waves can be viewed as Tollmien–Schlichting (TS) waves modified by the presence of wall waviness.

The range of corrugation wavenumbers α that leads to the instability giving rise to streamwise vortices is bounded from above and below. The most dangerous corrugation wavenumber, in the sense that it leads to the most amplified vortices, corresponds to $\alpha \approx 3$. The instability amplifies a continuous band of spanwise vortex wavenumbers μ . The most amplified vortex corresponds to $\mu \approx 2.15$. The range of unstable wave numbers α and μ increases with the increase of both the flow Reynolds numbers and the corrugation amplitude $2s$.

The disturbances in the form of travelling waves have a form very similar to TS waves. In the limit of zero corrugation amplitude, they reduce to TS waves. These waves are destabilized by the presence of wall corrugation, with the critical Reynolds number being reduced by about 10% in the range of parameters studied. This reduction is proportional to the amplitude of the corrugation. The amplification rates increase significantly with an increase of the corrugation amplitude $2s$.

For corrugation amplitude $2s > 0.014$, the vortex instability occurs at Reynolds numbers lower than those required for the initiation of the travelling wave instability. Since the presence of streamwise vortices is a strong harbinger of transition to turbulence, we are interested in determining the maximum corrugation amplitude that the flow can accommodate without inducing such vortices. It has been shown that the vortex instability does not occur if the roughness Reynolds $Re_r < 1.2$ in the range of parameters studied ($Re \leq 10^4$).

The authors would like to express their thanks to S. Krol and M. Floryan for carrying out computations and processing of the data. The authors would also like to thank P. J. D. Roberts for his assistance in the editing of this work. This research was supported by the Natural Science and Engineering Research Council of Canada (NSERC), Canadair and Bombardier de Havilland Inc.

Appendix A

$$\Delta = \frac{\partial^2}{\partial \xi^2} + 2a_{12}(\xi, \eta) \frac{\partial^2}{\partial \xi \partial \eta} + a_{22}(\xi, \eta) \frac{\partial^2}{\partial \eta^2} + a_2(\xi, \eta) \frac{\partial}{\partial \eta},$$

$$a_{12}(\xi, \eta) = -\frac{1}{h_U(\xi) - h_L(\xi)} \left[2 \frac{dh_U}{d\xi} + (\eta - 1) \left(\frac{dh_U}{d\xi} - \frac{dh_L}{d\xi} \right) \right],$$

$$a_{22}(\xi, \eta) = \frac{1}{(h_U(\xi) - h_L(\xi))^2} \left\{ \left[2 \frac{dh_U}{d\xi} + (\eta - 1) \left(\frac{dh_U}{d\xi} - \frac{dh_L}{d\xi} \right) \right]^2 + 4 \right\},$$

$$a_2(\xi, \eta) = -\frac{1}{(h_U(\xi) - h_L(\xi))^2} \left\{ \left[2 \frac{d^2 h_U}{d\xi^2} + (\eta - 1) \left(\frac{d^2 h_U}{d\xi^2} - \frac{d^2 h_L}{d\xi^2} \right) \right] \right.$$

$$\left. \times (h_U(\xi) - h_L(\xi)) - 2 \left[2 \frac{dh_U}{d\xi} + (\eta - 1) \left(\frac{dh_U}{d\xi} - \frac{dh_L}{d\xi} \right) \right] \left(\frac{dh_U}{d\xi} - \frac{dh_L}{d\xi} \right) \right\}.$$

Appendix B

$$\begin{aligned}
U_0 = & -\frac{(\eta-1)^2}{(1-\gamma)^3} \left(1 + B_0 + \frac{1}{4} \sum_{m=-\infty}^{+\infty} B_m B_{-m} \right) \\
& -\frac{(\eta-1)}{(1-\gamma)^3} \left(2 + B_0 + 2(A_0)_U + \sum_{m=-\infty}^{+\infty} B_m (A_{-m})_U \right) \\
& -2 \frac{(A_0)_U}{(1-\gamma)^3} - \frac{1}{(1-\gamma)^3} \sum_{m=-\infty}^{+\infty} (A_m)_U (A_{-m})_U - \frac{\gamma(2-\gamma)}{(1-\gamma)^3},
\end{aligned}$$

$$\begin{aligned}
U_n = & -\frac{(\eta-1)^2}{(1-\gamma)^3} \left(B_n + \frac{1}{4} \sum_{m=-\infty}^{+\infty} B_m B_{n-m} \right) \\
& -\frac{(\eta-1)}{(1-\gamma)^3} \left(B_n + 2(A_n)_U + \sum_{m=-\infty}^{+\infty} B_m (A_{n-m})_U \right) \\
& -2 \frac{(A_n)_U}{(1-\gamma)^3} - \frac{1}{(1-\gamma)^3} \sum_{m=-\infty}^{+\infty} (A_m)_U (A_{n-m})_U \quad (n \geq 1),
\end{aligned}$$

$$\begin{aligned}
\hat{\Psi}_0 = & -\frac{(\eta-1)^3}{24(1-\gamma)^3} \left(8 + 12B_0 + 6 \sum_{m=-\infty}^{+\infty} B_m B_{-m} + \sum_{k=-\infty}^{+\infty} \sum_{m=-\infty}^{+\infty} B_k B_m B_{-k-m} \right) \\
& -\frac{(\eta-1)^2}{4(1-\gamma)^3} \left(4 + 4B_0 + \sum_{m=-\infty}^{+\infty} B_m B_{-m} + 4(A_0)_U + 4 \sum_{m=-\infty}^{+\infty} B_m (A_{-m})_U \right. \\
& \left. + \sum_{k=-\infty}^{+\infty} \sum_{m=-\infty}^{+\infty} B_k B_m (A_{-k-m})_U \right) - \frac{(\eta-1)}{2(1-\gamma)^3} \left(\gamma(2-\gamma)(2+B_0) + 4(A_0)_U \right. \\
& \left. + 2 \sum_{m=-\infty}^{+\infty} (A_m)_U (A_{-m})_U + 2 \sum_{m=-\infty}^{+\infty} B_m (A_{-m})_U + \sum_{k=-\infty}^{+\infty} \sum_{m=-\infty}^{+\infty} B_k (A_m)_U (A_{-k-m})_U \right) \\
& + \frac{2}{3} + \frac{1}{3(1-\gamma)^3} (2 - 6\gamma + 3\gamma^2) - \frac{\gamma(2-\gamma)}{(1-\gamma)^3} (A_0)_U \\
& - \frac{1}{(1-\gamma)^3} \sum_{m=-\infty}^{+\infty} (A_m)_U (A_{-m})_U - \frac{1}{3(1-\gamma)^3} \sum_{k=-\infty}^{+\infty} \sum_{m=-\infty}^{+\infty} (A_k)_U (A_m)_U (A_{-k-m})_U,
\end{aligned}$$

$$\begin{aligned}
\hat{\Psi}_n = & -\frac{(\eta-1)^3}{24(1-\gamma)^3} \left(12B_n + 6 \sum_{m=-\infty}^{+\infty} B_m B_{n-m} + \sum_{k=-\infty}^{+\infty} \sum_{m=-\infty}^{+\infty} B_k B_m B_{n-k-m} \right) \\
& -\frac{(\eta-1)^2}{4(1-\gamma)^3} \left(4B_n + \sum_{m=-\infty}^{+\infty} B_m B_{n-m} + 4(A_n)_U + 4 \sum_{m=-\infty}^{+\infty} B_m (A_{n-m})_U \right. \\
& \left. + \sum_{k=-\infty}^{+\infty} \sum_{m=-\infty}^{+\infty} B_k B_m (A_{n-k-m})_U \right) - \frac{(\eta-1)}{2(1-\gamma)^3} \left(\gamma(2-\gamma)B_n + 4(A_n)_U \right. \\
& \left. + 2 \sum_{m=-\infty}^{+\infty} (A_m)_U (A_{n-m})_U + 2 \sum_{m=-\infty}^{+\infty} B_m (A_{n-m})_U + \sum_{k=-\infty}^{+\infty} \sum_{m=-\infty}^{+\infty} B_k (A_m)_U (A_{n-k-m})_U \right) \\
& - \frac{\gamma(2-\gamma)}{(1-\gamma)^3} (A_n)_U - \frac{1}{(1-\gamma)^3} \sum_{m=-\infty}^{+\infty} (A_m)_U (A_{n-m})_U \\
& - \frac{1}{3(1-\gamma)^3} \sum_{k=-\infty}^{+\infty} \sum_{m=-\infty}^{+\infty} (A_k)_U (A_m)_U (A_{n-k-m})_U \quad (n \geq 1),
\end{aligned}$$

where $B_n = (A_n)_U - (A_n)_L$.

Appendix C

Differential equations for Φ_n in (2.18) for the upper and lower walls given by (2.23) have the following form

$$\begin{aligned}
& \mathcal{K}_{4,n} \Phi_{n+4} + \mathcal{K}_{3,n} \Phi_{n+3} + \mathcal{K}_{2,n} \Phi_{n+2} + \mathcal{K}_{1,n} \Phi_{n+1} + \mathcal{K}_{0,n} \Phi_n + \mathcal{K}_{-1,n} \Phi_{n-1} \\
& + \mathcal{K}_{-2,n} \Phi_{n-2} + \mathcal{K}_{-3,n} \Phi_{n-3} + \mathcal{K}_{-4,n} \Phi_{n-4} - i\alpha \text{Re} \sum_{l=-\infty}^{+\infty} U_{n-l} \\
& \times (\mathcal{L}_{3,l} \Phi_{l+3} + \mathcal{L}_{2,l} \Phi_{l+2} + \mathcal{L}_{1,l} \Phi_{l+1} + \mathcal{L}_{0,l} \Phi_l + \mathcal{L}_{-1,l} \Phi_{l-1} + \mathcal{L}_{-2,l} \Phi_{l-2} \\
& + \mathcal{L}_{-3,l} \Phi_{l-3}) + i\alpha \text{Re} \sum_{l=-\infty}^{+\infty} \frac{d^2 U_{n-l}}{d\eta^2} (\mathcal{H}_{1,l} \Phi_{l+1} + \mathcal{H}_{0,l} \Phi_l + \mathcal{H}_{-1,l} \Phi_{l-1}) + i\alpha \text{Re} \\
& \times \sum_{l=-\infty}^{+\infty} \left[(n-l) \Phi_{n-l} (\mathcal{M}_{2,l} \Phi_{l+2} + \mathcal{M}_{1,l} \Phi_{l+1} + \mathcal{M}_{0,l} \Phi_l + \mathcal{M}_{-1,l} \Phi_{l-1} + \mathcal{M}_{-2,l} \Phi_{l-2}) \right. \\
& \left. + l \frac{d\Phi_{n-l}}{d\eta} (\mathcal{N}_{2,l} \Phi_{l+2} + \mathcal{N}_{1,l} \Phi_{l+1} + \mathcal{N}_{0,l} \Phi_l + \mathcal{N}_{-1,l} \Phi_{l-1} + \mathcal{N}_{-2,l} \Phi_{l-2}) \right] = 0,
\end{aligned} \tag{C1}$$

where the linear differential operators \mathcal{K} , \mathcal{L} , \mathcal{H} , \mathcal{M} and \mathcal{N} are given below. The corresponding boundary conditions at $\eta = \pm 1$ have the form

$$\frac{d\Phi_0}{d\eta} = \frac{2s^2}{(1-\gamma)^2}, \tag{C2}$$

$$\Phi_1 = \frac{s^3}{(1-\gamma)^3}, \quad \frac{d\Phi_1}{d\eta} = \pm \frac{2s}{1-\gamma}, \tag{C3}$$

$$\Phi_2 = \pm \frac{s^2}{(1-\gamma)^2}, \quad \frac{d\Phi_2}{d\eta} = \frac{s^2}{(1-\gamma)^2}, \quad (C4)$$

$$\Phi_3 = \frac{1}{3} \frac{s^3}{(1-\gamma)^3}, \quad \frac{d\Phi_n}{d\eta} = 0 \quad (n \geq 3), \quad (C5)$$

$$\Phi_n = 0 \quad (n \geq 4). \quad (C6)$$

and are supplemented by the fixed volume flux conditions in the form

$$\Phi_0(-1) = 0, \quad \Phi_0(1) = \frac{4s^2}{(1-\gamma)^2}, \quad (C7)$$

where

$$\mathcal{H}_{4,n} = \frac{\alpha^4 s^4}{(1-\gamma)^4} \frac{d^4}{d\eta^4}, \quad \mathcal{H}_{3,n} = \alpha^3 s^3 \frac{2\alpha(2n+3)}{(1-\gamma)^3} \frac{d^3}{d\eta^3},$$

$$\mathcal{H}_{2,n} = \alpha^2 s^2 \left\{ -2 \frac{(2\alpha^2 s^2 + 1)}{(1-\gamma)^4} \frac{d^4}{d\eta^4} + \frac{\alpha^2(6n^2 + 12n + 7)}{(1-\gamma)^2} \frac{d^2}{d\eta^2} \right\},$$

$$\mathcal{H}_{1,n} = s(3\alpha^2 s^2 + 1) \left[\frac{-2\alpha^2(2n+1)}{(1-\gamma)^3} \right] \frac{d^3}{d\eta^3} + \alpha^3 s \left[\frac{\alpha(4n^3 + 6n^2 + 4n + 1)}{(1-\gamma)} \right] \frac{d}{d\eta},$$

$$\mathcal{H}_{0,n} = \left[\frac{2\alpha^2 s^2(3\alpha^2 s^2 + 2) + 1}{(1-\gamma)^4} \right] \frac{d^4}{d\eta^4} + \left[\frac{-2\alpha^4 s^2(6n^2 + 1)}{(1-\gamma)^2} - \frac{2\alpha^2 n^2}{(1-\gamma)^2} \right] \frac{d^2}{d\eta^2} + \alpha^4 n^4,$$

$$\mathcal{H}_{-1,n} = s(3\alpha^2 s^2 + 1) \left[\frac{2\alpha^2(2n-1)}{(1-\gamma)^3} \right] \frac{d^3}{d\eta^3} - \alpha^3 s \left[\frac{\alpha(4n^3 - 6n^2 + 4n - 1)}{(1-\gamma)} \right] \frac{d}{d\eta},$$

$$\mathcal{H}_{-2,n} = \alpha^2 s^2 \left\{ \frac{-2(2\alpha^2 s^2 + 1)}{(1-\gamma)^4} \frac{d^4}{d\eta^4} + \frac{\alpha^2(6n^2 - 12n + 7)}{(1-\gamma)^2} \frac{d^2}{d\eta^2} \right\},$$

$$\mathcal{H}_{-3,n} = -\alpha^3 s^3 \frac{2\alpha(2n-3)}{(1-\gamma)^3} \frac{d^3}{d\eta^3}, \quad \mathcal{H}_{-4,n} = \frac{\alpha^4 s^4}{(1-\gamma)^4} \frac{d^4}{d\eta^4},$$

$$\mathcal{L}_{3,l} = -\frac{\alpha^2 s^3}{(1-\gamma)^3} \frac{d^3}{d\eta^3}, \quad \mathcal{L}_{2,l} = -\frac{3\alpha^2 s^2(l+1)}{(1-\gamma)^2} \frac{d^2}{d\eta^2},$$

$$\mathcal{L}_{1,l} = \frac{s(3\alpha^2 s^2 + 1)}{(1-\gamma)^3} \frac{d^3}{d\eta^3} - \frac{\alpha^2 s(3l^2 + 3l + 1)}{(1-\gamma)} \frac{d}{d\eta},$$

$$\mathcal{L}_{0,l} = \frac{l(6\alpha^2 s^2 + 1)}{(1-\gamma)^2} \frac{d^2}{d\eta^2} - \alpha^2 l^3,$$

$$\mathcal{L}_{-1,l} = -\frac{s(3\alpha^2 s^2 + 1)}{(1-\gamma)^3} \frac{d^3}{d\eta^3} + \frac{\alpha^2 s(3l^2 - 3l + 1)}{(1-\gamma)} \frac{d}{d\eta},$$

$$\mathcal{L}_{-2,l} = -\frac{3\alpha^2 s^2(l-1)}{(1-\gamma)^2} \frac{d^2}{d\eta^2}, \quad \mathcal{L}_{-3,l} = \frac{\alpha^2 s^3}{(1-\gamma)^3} \frac{d^3}{d\eta^3},$$

$$\begin{aligned}\mathcal{H}_{1,l} &= \frac{s}{(1-\gamma)^3} \frac{d}{d\eta}, & \mathcal{H}_{0,l} &= \frac{l}{(1-\gamma)^2}, & \mathcal{H}_{-1,l} &= -\frac{s}{(1-\gamma)^3} \frac{d}{d\eta}, \\ \mathcal{M}_{2,l} &= -\frac{\alpha^2 s^2}{(1-\gamma)^3} \frac{d^3}{d\eta^3}, & \mathcal{M}_{1,l} &= -\frac{\alpha^2 s(2l+1)}{(1-\gamma)^2} \frac{d^2}{d\eta^2}, \\ \mathcal{M}_{0,l} &= \frac{(2\alpha^2 s^2 + 1)}{(1-\gamma)^3} \frac{d^3}{d\eta^3} - \frac{\alpha^2 l^2}{(1-\gamma)} \frac{d}{d\eta}, \\ \mathcal{M}_{-1,l} &= \frac{\alpha^2 s(2l-1)}{(1-\gamma)^2} \frac{d^2}{d\eta^2}, & \mathcal{M}_{-2,l} &= -\frac{\alpha^2 s^2}{(1-\gamma)^3} \frac{d^3}{d\eta^3}, \\ \mathcal{N}_{2,l} &= \frac{\alpha^2 s^2}{(1-\gamma)^3} \frac{d^2}{d\eta^2}, & \mathcal{N}_{1,l} &= \frac{\alpha^2 s(2l+1)}{(1-\gamma)^2} \frac{d}{d\eta}, \\ \mathcal{N}_{0,l} &= -\frac{(2\alpha^2 s^2 + 1)}{(1-\gamma)^3} \frac{d^2}{d\eta^2} + \frac{\alpha^2 l^2}{(1-\gamma)}, \\ \mathcal{N}_{-1,l} &= -\frac{\alpha^2 s(2l-1)}{(1-\gamma)^2} \frac{d}{d\eta}, & \mathcal{N}_{-2,l} &= \frac{\alpha^2 s^2}{(1-\gamma)^3} \frac{d^2}{d\eta^2}.\end{aligned}$$

Appendix D

$$\begin{aligned}\frac{\partial \theta_3}{\partial t} + u_2 \left(\frac{\partial \theta_3}{\partial \xi} - \frac{h_\xi}{1-\gamma} \frac{\partial \theta_3}{\partial \eta} \right) - \phi_2 \frac{\partial u_3}{\partial \zeta} + \frac{v_2}{1-\gamma} \frac{\partial \theta_3}{\partial \eta} \\ - \theta_3 \left(\frac{\partial u_2}{\partial \xi} - \frac{h_\xi}{1-\gamma} \frac{\partial u_2}{\partial \eta} \right) - \frac{\psi_3}{1-\gamma} \frac{\partial u_2}{\partial \eta} = \frac{1}{Re} \Delta \theta_3, \quad (D 1)\end{aligned}$$

$$\begin{aligned}\frac{\partial \phi_3}{\partial t} + u_2 \left(\frac{\partial \phi_3}{\partial \xi} - \frac{h_\xi}{1-\gamma} \frac{\partial \phi_3}{\partial \eta} \right) - \phi_2 \frac{\partial w_3}{\partial \zeta} + \frac{v_2}{1-\gamma} \frac{\partial \phi_3}{\partial \eta} \\ + u_3 \left(\frac{\partial \phi_2}{\partial \xi} - \frac{h_\xi}{1-\gamma} \frac{\partial \phi_2}{\partial \eta} \right) + \frac{v_3}{1-\gamma} \frac{\partial \phi_2}{\partial \eta} = \frac{1}{Re} \Delta \phi_3, \quad (D 2)\end{aligned}$$

$$\begin{aligned}\frac{\partial \psi_3}{\partial t} + u_2 \left(\frac{\partial \psi_3}{\partial \xi} - \frac{h_\xi}{1-\gamma} \frac{\partial \psi_3}{\partial \eta} \right) - \phi_2 \frac{\partial v_3}{\partial \zeta} + \frac{v_2}{1-\gamma} \frac{\partial \psi_3}{\partial \eta} \\ - \theta_3 \left(\frac{\partial v_2}{\partial \xi} - \frac{h_\xi}{1-\gamma} \frac{\partial v_2}{\partial \eta} \right) - \frac{\psi_3}{1-\gamma} \frac{\partial v_2}{\partial \eta} = \frac{1}{Re} \Delta \psi_3, \quad (D 3)\end{aligned}$$

$$\frac{\partial u_3}{\partial \xi} - \frac{h_\xi}{1-\gamma} \frac{\partial u_3}{\partial \eta} + \frac{\partial w_3}{\partial \zeta} + \frac{1}{1-\gamma} \frac{\partial v_3}{\partial \eta} = 0, \quad (D 4)$$

where

$$\Delta = \frac{\partial^2}{\partial \xi^2} - \frac{2h_\xi}{1-\gamma} \frac{\partial^2}{\partial \xi \partial \eta} + \frac{\partial^2}{\partial \zeta^2} + \frac{1+h_\xi^2}{(1-\gamma)^2} \frac{\partial^2}{\partial \eta^2} - \frac{h_{\xi\xi}}{1-\gamma} \frac{\partial}{\partial \eta}. \quad (D 5)$$

The mean flow satisfies the following equations

$$u_2 \left(\frac{\partial \phi_2}{\partial \xi} - \frac{h_\xi}{1-\gamma} \frac{\partial \phi_2}{\partial \eta} \right) + \frac{v_2}{1-\gamma} \frac{\partial \phi_2}{\partial \eta} = \frac{1}{Re} \Delta \phi_2, \quad (\text{D } 6)$$

$$\frac{\partial u_2}{\partial \xi} - \frac{h_\xi}{1-\gamma} \frac{\partial u_2}{\partial \eta} + \frac{1}{1-\gamma} \frac{\partial v_2}{\partial \eta} = 0. \quad (\text{D } 7)$$

Appendix E

$$\begin{aligned} & A_u^{(m)} \mathbf{g}_u^{(m)} + A_w^{(m)} \mathbf{g}_w^{(m)} + A_v^{(m)} \mathbf{g}_v^{(m)} \\ &= -(G_u^{(m)} \mathbf{g}_u^{(m-5)} + G_v^{(m)} \mathbf{g}_v^{(m-5)} + H_u^{(m)} \mathbf{g}_u^{(m-4)} + H_w^{(m)} \mathbf{g}_w^{(m-4)} + H_v^{(m)} \mathbf{g}_v^{(m-4)} \\ & \quad + I_u^{(m)} \mathbf{g}_u^{(m-3)} + I_w^{(m)} \mathbf{g}_w^{(m-3)} + I_v^{(m)} \mathbf{g}_v^{(m-3)} + J_u^{(m)} \mathbf{g}_u^{(m-2)} + J_w^{(m)} \mathbf{g}_w^{(m-2)} \\ & \quad + J_v^{(m)} \mathbf{g}_v^{(m-2)} + K_u^{(m)} \mathbf{g}_u^{(m-1)} + K_w^{(m)} \mathbf{g}_w^{(m-1)} + K_v^{(m)} \mathbf{g}_v^{(m-1)} + L_u^{(m)} \mathbf{g}_u^{(m+1)} \\ & \quad + L_w^{(m)} \mathbf{g}_w^{(m+1)} + L_v^{(m)} \mathbf{g}_v^{(m+1)} + M_u^{(m)} \mathbf{g}_u^{(m+2)} + M_w^{(m)} \mathbf{g}_w^{(m+2)} + M_v^{(m)} \mathbf{g}_v^{(m+2)} \\ & \quad + N_u^{(m)} \mathbf{g}_u^{(m+3)} + N_w^{(m)} \mathbf{g}_w^{(m+3)} + N_v^{(m)} \mathbf{g}_v^{(m+3)} + Q_u^{(m)} \mathbf{g}_u^{(m+4)} \\ & \quad + Q_w^{(m)} \mathbf{g}_w^{(m+4)} + Q_v^{(m)} \mathbf{g}_v^{(m+4)} + R_u^{(m)} \mathbf{g}_u^{(m+5)} + R_v^{(m)} \mathbf{g}_v^{(m+5)}), \end{aligned} \quad (\text{E } 1)$$

$$\begin{aligned} & B_u^{(m)} \mathbf{g}_u^{(m)} + B_w^{(m)} \mathbf{g}_w^{(m)} + B_v^{(m)} \mathbf{g}_v^{(m)} \\ &= -(\mathcal{H}_u^{(m)} \mathbf{g}_u^{(m-4)} + \mathcal{H}_v^{(m)} \mathbf{g}_v^{(m-4)} + \mathcal{J}_u^{(m)} \mathbf{g}_u^{(m-3)} + \mathcal{J}_w^{(m)} \mathbf{g}_w^{(m-3)} \\ & \quad + \mathcal{J}_v^{(m)} \mathbf{g}_v^{(m-3)} + \mathcal{J}_u^{(m)} \mathbf{g}_u^{(m-2)} + \mathcal{J}_w^{(m)} \mathbf{g}_w^{(m-2)} + \mathcal{J}_v^{(m)} \mathbf{g}_v^{(m-2)} \\ & \quad + \mathcal{K}_u^{(m)} \mathbf{g}_u^{(m-1)} + \mathcal{K}_w^{(m)} \mathbf{g}_w^{(m-1)} + \mathcal{K}_v^{(m)} \mathbf{g}_v^{(m-1)} + \mathcal{L}_u^{(m)} \mathbf{g}_u^{(m+1)} \\ & \quad + \mathcal{L}_w^{(m)} \mathbf{g}_w^{(m+1)} + \mathcal{L}_v^{(m)} \mathbf{g}_v^{(m+1)} + \mathcal{M}_u^{(m)} \mathbf{g}_u^{(m+2)} + \mathcal{M}_w^{(m)} \mathbf{g}_w^{(m+2)} \\ & \quad + \mathcal{M}_v^{(m)} \mathbf{g}_v^{(m+2)} + \mathcal{N}_u^{(m)} \mathbf{g}_u^{(m+3)} + \mathcal{N}_w^{(m)} \mathbf{g}_w^{(m+3)} + \mathcal{N}_v^{(m)} \mathbf{g}_v^{(m+3)} \\ & \quad + \mathcal{Q}_u^{(m)} \mathbf{g}_u^{(m+4)} + \mathcal{Q}_v^{(m)} \mathbf{g}_v^{(m+4)}), \end{aligned} \quad (\text{E } 2)$$

$$it_m \mathbf{g}_u^{(m)} + i\mu \mathbf{g}_w^{(m)} + \frac{1}{1-\gamma} \frac{d}{d\eta} \mathbf{g}_v^{(m)} - \frac{izs}{1-\gamma} \frac{d}{d\eta} (\mathbf{g}_u^{(m-1)} - \mathbf{g}_u^{(m+1)}) = 0. \quad (\text{E } 3)$$

All differential operators in the above equations are linear. Their explicit form is omitted from this presentation owing to excessive length requirements (60 pages). Details can be found in Cabal (1998).

REFERENCES

- BECHERT, D. W. 1987 Experiments on three dimensional riblets. *Turbulent Drag Reduction by Passive Means*. Royal Aeronautical Society, London.
- BOYD, J. P. 1988 Chebyshev and Fourier Spectral Methods. Springer, New York.
- CABAL, A. 1998 Stability of wall-bounded flow modified due to the presence of distributed surface roughness. PhD thesis, The University of Western Ontario, London, Ontario, Canada.
- CABAL, A., SZUMBARSKI, J. & FLORYAN J. M. 2001 Numerical simulation of flows over corrugated walls. *Comput. Fluids*, **30**, 753–776.
- CANUTO, C., HUSSAINI, M. Y., QUARTERONI, A. & ZANG, T. 1988 Spectral Methods in Fluid Dynamics. Springer, New York.

- CASH, J. R. & WRIGHT M. H. 1991 A deferred correction method for nonlinear two-point boundary value problems: implementation and numerical evaluation. *SIAM J. Sci. Stat. Comput.* **12**, 971–989.
- CHU, D. C. & KARNIADAKIS, G. E. 1993 A direct numerical simulation of laminar and turbulent flow over riblet-mounted surfaces. *J. Fluid Mech.* **250**, 1–42.
- CORKE, T. C., BAR SEVER, A. & MORKOVIN M. V. 1986 Experiments on transition enhancement by distributed surface roughness. *Phys. Fluids* **29**, 3199–3213.
- FEINDT, E. G. 1956 Untersuchungen über die Abhängigkeit des Umschlages laminar-turbulent von der Oberflächenrauigkeit und der Druckverteilung. *Jahrbuch 1956 der Schiffbautechnischen Gesellschaft*, **50**, 180–203.
- FLORYAN, J. M. 1997 Stability of wall-bounded shear layers in the presence of simulated distributed surface roughness. *J. Fluid Mech.* **335**, 29–55.
- FLORYAN, J. M., YAMAMOTO, K. & MURASE, T. 1992 Laminar–turbulent transition in the presence of simulated wall roughness. *Can. Aeronaut. & Space J.* **38**, 173–182.
- FORNBERG, B. 1996 *A Practical Guide to Pseudospectral Methods*. Cambridge University Press.
- GOTTLIEB, D. & ORSZAG, S. A. 1977 *Numerical Analysis of Spectral Methods*. SIAM, Philadelphia.
- KENDALL, J. M. 1981 Laminar boundary layer distortion by surface roughness, effect upon stability. *AIAA Paper* 81-0195.
- PEREYRA, V. 1979 PASVA3: An adaptive finite–difference Fortran program for first order nonlinear, ordinary boundary problems. In *Codes for Boundary Value Problems in Ordinary Differential Equations*. Lecture Notes in Computer Science, vol. 76, pp. 67–88. Springer.
- RESHOTKO, E. 1984 Disturbances in a laminar boundary layer due to distributed surface roughness. In *Turbulence and Chaotic Phenomena. Proc. of IUTAM Symp.* (ed. T. Tatsumi), pp. 39–46. Elsevier.
- RESHOTKO, E. & LEVENTHAL, L. 1981 Preliminary experimental study of disturbances in laminar boundary layers due to distributed surface roughness. *AIAA Paper* 81-1224.
- SCHMID, P. J. & HENNINGSON, D. S. 2001 *Stability and Transition in Shear Flows*. Springer.
- TANG, T. 1994 Lecture notes: A graduate course on spectral methods for differential equations. <http://www.math.sfu.ca/~tangtao/spectral.html>, Simon Fraser University, Vancouver, BC.